



HAL
open science

Naphthyl-fused phosphepines: Luminescent contorted polycyclic P-heterocycles

Thomas Delouche, Réka Mokrai, Thierry Roisnel, Denis Tondelier, Bernard Geffroy, László Nyulászi, Zoltán Benkő, Muriel Hissler, Pierre-Antoine Bouit

► **To cite this version:**

Thomas Delouche, Réka Mokrai, Thierry Roisnel, Denis Tondelier, Bernard Geffroy, et al.. Naphthyl-fused phosphepines: Luminescent contorted polycyclic P-heterocycles. *Chemistry - A European Journal*, 2020, 26 (8), pp.1856 -1863. 10.1002/chem.201904490 . hal-02394493

HAL Id: hal-02394493

<https://hal.science/hal-02394493>

Submitted on 4 Dec 2019

HAL is a multi-disciplinary open access archive for the deposit and dissemination of scientific research documents, whether they are published or not. The documents may come from teaching and research institutions in France or abroad, or from public or private research centers.

L'archive ouverte pluridisciplinaire **HAL**, est destinée au dépôt et à la diffusion de documents scientifiques de niveau recherche, publiés ou non, émanant des établissements d'enseignement et de recherche français ou étrangers, des laboratoires publics ou privés.

Naphthyl-fused phosphepines: Luminescent contorted polycyclic P-heterocycles

Thomas Delouche,^[a] Réka Mokrai,^[a,b] Thierry Roisnel,^[a] Denis Tondelier,^[c] Bernard Geffroy,^[d] László Nyulászi,^[b,e] Zoltán Benkő,^{*[b]} Muriel Hissler^{*[a]} and Pierre-Antoine Bouit^{*[a]}

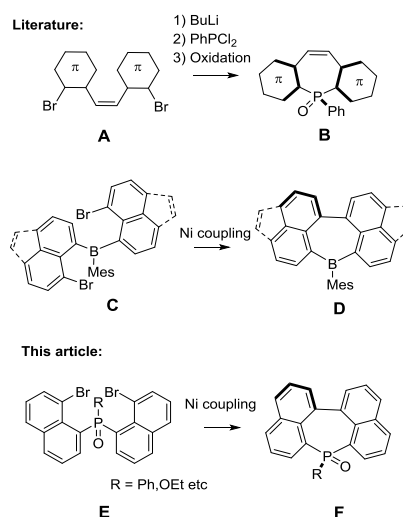
Dedicated to J. –F. Halet on the occasion of his 60th birthday

Abstract: The article presents the synthesis of a new family of naphthyl-fused phosphepines through Ni-mediated C-C coupling. Interestingly, the chloro-phosphine-oxide intermediate shows strong resistance toward oxidation/hydrolysis due to a combination of steric hindrance and pnictogen interactions. However, it can undergo substitution reactions under specific conditions. The optical / redox properties and the electronic structure of these new π -systems were studied experimentally (UV-vis absorption, emission, cyclic voltammetry) and computationally (TD-DFT calculations, NICS investigation). Taking advantage of the luminescence of these derivatives, a blue emitting OLED has been prepared highlighting that these novel π -conjugated P-heterocycles appear as promising building blocks for solid-state lighting applications.

Introduction

During the last two decades, the research on phosphorus-containing π -conjugated systems based on small molecules, oligomers and polymers has increased substantially thanks to the development of "plastic electronic" devices.^[1] Compared to purely organic π -systems, the presence of a heteroatom such as phosphorus affords multiple molecular engineering strategies in order to tune the chemical structure and the physico-chemical properties. Indeed, the P-atom can be involved in various bonding situations (σ^3, λ^3 -phosphane, σ^2, λ^3 -phosphaalkene, σ^4, λ^5 -phosphorus ylide etc), which strongly impacts the nature of the delocalization in the corresponding π -system.^[2] Furthermore, the specific reactivity of the σ^3, λ^3 -P-atom affords an almost unlimited way of tuning its properties.^[3] Among these strategies, introducing the P-center into an unsaturated ring is also an excellent way to

modify the properties of the corresponding π -system. Phosphole, the P-analogue of thiophene, is by far the most studied P-heterocycle based π -system from the point of view of its reactivity as well as for its introduction into devices (light-emitting diodes, solar cells, batteries...)^[4] However, P-heterocycles are not limited to the phosphole family and during the last few years, other π -systems based on phosphetenes (4-membered unsaturated P-ring),^[5] phosphaphenalenenes / phosphinines (6-membered P-ring)^[6] or phosphepines (7 membered P-rings)^[7] have started to be studied in the context of molecular materials. The phosphepine ring caught our attention as it displays the most distorted framework among these conjugated heterocycles, which may strongly impact the physico-chemical properties. In particular, we and others studied non-planar diarylophosphepines (**B**, Scheme 1) showing tunable optical/redox properties and promising activity in field-effect transistors.^[8] Those diarylophosphepines are usually synthesized according to a classical sequence of dilithiation of a dibromoaryl then reaction with a dichlorophosphine (Scheme 1). In order to develop a new family of π -extended phosphepine, we decided to adapt the Ni-mediated coupling strategy that allowed M. Wagner *et al* to prepare distorted borepins **D** and thus investigate the effect of the insertion of a P-atom into such quadruply-fused phosphepine **F** (Scheme 1).^[9]



Scheme 1. Reported access to π -extended phosphepine (**B**), π -extended borepin (**D**) and synthetic strategy employed in this article.

In this article, we present the synthesis of a new family of naphthyl-fused phosphepines. The optical and redox properties

[a] T. Delouche, R. Mokrai, T. Roisnel, Prof. M. Hissler, Dr P.-A. Bouit Univ Rennes, CNRS, ISCR - UMR 6226, F-35000 Rennes. E-mail: muriel.hissler@univ-rennes1.fr, pierre-antoine.bouit@univ-rennes1.fr

[b] Department of Inorganic and Analytical Chemistry, Budapest University of Technology and Economics Szt. Gellert ter 4 H-1111 Budapest, Hungary E-mail: zbenko@mail.bme.hu

[c] LPICM, CNRS, Ecole Polytechnique, IPParis, 91128 Palaiseau, France

[d] LICSEN, NIMBE, CEA, CNRS, Université Paris-Saclay, CEA Saclay, 91191 Gif-sur-Yvette Cedex, France

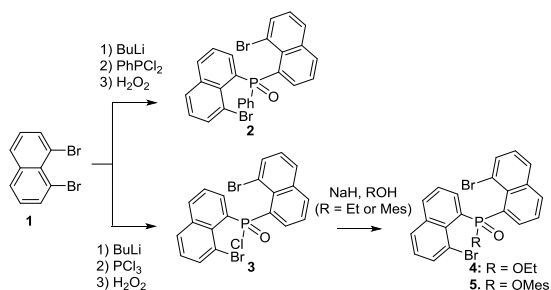
[e] MTA-BME Computation Driven Chemistry Research Group. Szt. Gellert ter 4 H-1111 Budapest, Hungary E-mail: nyulaszi@mail.bme.hu

and the electronic structure of these new π -systems have been studied experimentally and computationally. Incorporation of one of these molecules into an OLED device has also been performed.

Results and Discussion

Synthesis and structural study of precursors

Based on our synthetic strategy toward **F** (Scheme 1), the first step of our approach was the preparation of the bromonaphthylphosphine-oxide **E**. The reaction between 1,8-dibromonaphthalene **1** and BuLi followed by *in situ* addition of dichlorophenylphosphine and subsequent oxidation afforded quantitatively a product characterized by a single peak in the ^{31}P NMR spectrum ($\delta = +42.9$ ppm) and broad multiplets in the ^1H NMR (Fig. S8). This can easily be interpreted considering the presence of interconverting rotamers at room temperature (rt). Indeed, the signals in the ^1H NMR sharpened upon cooling the temperature to 243K (Fig. S8).^[9] The product was unambiguously characterized as **2** by its crystallographic structure (Scheme 2 and Fig. 1). The molecular structure of **2** displays high steric hindrance with torsion of the naphthyl ring as well as presence of intramolecular contacts shorter than the sum of van der Waals radii (d_{vdW}) between O and Br ($3.122(1) \text{ \AA} < d_{\text{OBr}} < 3.144(2) \text{ \AA}$, see Fig 1, $d_{\text{vdW}}(\text{O-Br})=3.37 \text{ \AA}$) and especially between P and Br centers ($3.323(1) \text{ \AA} < d_{\text{PBr}} < 3.325(1) \text{ \AA}$, see Fig 1, $d_{\text{vdW}}(\text{P-Br})=3.65 \text{ \AA}$). This sterically crowded structure with intramolecular interactions is in accord with the presence of interconverting rotamers at rt.



Scheme 2. Synthesis of bromonaphthyl substituted phosphine oxide **2-4**.

The same sequence was then performed using PCl_3 as starting phosphine and the product identified after oxidation was the chlorophosphine oxide **3** (Scheme 2). This compound displays similar NMR behaviour as **2** with broad ^1H signals that resolved upon cooling to temperature (Fig. S9). Furthermore, X-ray diffraction allowed the unambiguous characterization of **3** (Fig. 1). The high steric hindrance around the P-atom combined with the presence of intramolecular short contacts ($3.204(1) \text{ \AA} < d_{\text{OBr}} < 3.300(2) \text{ \AA}$, $3.246(1) \text{ \AA} < d_{\text{PBr}} < 3.399(1) \text{ \AA}$, Fig 1) probably allows sterically protecting the P-Cl bond making **3** fully air and moisture stable. This is surprising because chlorophosphine-oxides are usually highly sensitive to hydrolysis.^[10] Nevertheless, the Cl atom of **3** could be substituted by strong nucleophiles

alkoxides/aryloxides to afford **4** and **5** (Scheme 2). Their structures could be confirmed by X-ray diffraction (Fig S13-14).

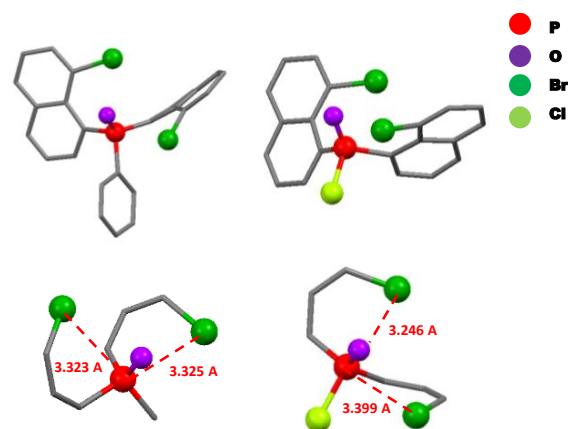
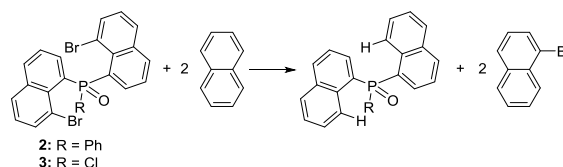


Figure 1: Depictions of the X-ray crystal structures of **2** (left) and **3** (right) (top) with zooms on the P environment with measured P-Br distances (red dotted line) (bottom). Hydrogen atoms were omitted for clarity.

In order to gain more insight into the possible rotamers and the nature of the weak interactions, we have performed DFT calculations at different levels, here only the results obtained at the B3LYP-D3/6-31+G* level are discussed. In the case of **2** two local minima with the same energy were found on the potential energy surface and the corresponding structures show enantiomeric relation (Fig. S32-33). The transition state connecting these enantiomers (Fig. S31) was also located and the interconversion barrier is $\Delta E^\ddagger=15.8$ kcal/mol. Similarly, an interconversion barrier of $\Delta E^\ddagger=12.3$ kcal/mol has been obtained for compound **3** (for details see ESI). Therefore, at low temperature both enantiomers are present. However, they can interconvert into each other at rt resulting in broad resonances. At higher temperature, the substituents freely rotate around the C-P bonds and sharp signals resulting from an average of the interconverting structures are observed. To estimate the energetic stabilization caused by the weak interactions, the isodesmic reaction depicted in Scheme 3 has been calculated for compounds **2** and **3**. Remarkable stabilization reaching 18.5 kcal/mol is found in **3**, while somewhat smaller but still significant value of 14.8 kcal/mol is obtained for **2**. These isodesmic stabilization energies are in the range of the above discussed interconversion barriers. Thus, in the transition state these weak interactions are disrupted.



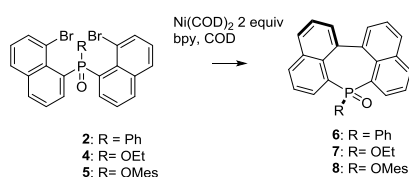
Scheme 3. Isodesmic reactions for estimation of the stabilization effects of secondary interactions.

The covalent character of possible $\text{P}\cdots\text{Br}$ and $\text{O}\cdots\text{Br}$ interactions has been assessed employing Wiberg Bond Indices (WBI). This shows practically no interaction between the O and Br centers (WBI: ~ 0.007), whereas the ~ 0.02 WBI value for both P-Br pairs may indicate pnictogen interaction between P and Br.^[11-12] The

presence of weak interactions between the P and Br atoms is further corroborated by an atom in molecules (AIM) analysis of the electron density (see ESI, Fig S35). A bond critical point (BCP) can be found between the Br and the P–O vector, and the properties of this BCP are in line with those observed for pnictogen interactions (low electron density, positive Laplacian of the electron density, positive total electronic energy density).^[13] In conclusion, a weak pnictogen interaction between P and Br may contribute to the particular stability of **3**, that can be easily handled in air and purified with classical chromatography techniques.

Synthesis and structural study of naphthyl-fused phosphepines

The fusing step toward **F** (Scheme 1) was then tested employing the Yamamoto-type conditions optimized by Wagner *et al.*^[9] (using 2 equiv. of Ni(COD)₂, COD (2 equiv.) and bpy in THF) allowed us to convert **2** into **6** (³¹P NMR: $\delta = +22.7$ ppm) in good yields (75%) (Scheme 4). **6** was characterized by multinuclear NMR, HRMS and X-ray diffraction (Fig. 2). Based on these results, the Ni-mediated coupling was used to prepare **7-8** in good yields (75% and 47%, respectively). These examples show that the Yamamoto-type reaction is an efficient way to prepare unprecedented naphthyl-fused phosphepines from the corresponding bromo-naphthylphosphines. As expected for contorted polycyclic aromatic systems, the solubility of these compounds in most organic solvents such as DCM, AcOEt, or THF is rather good.



Scheme 4. Synthesis of naphthyl-fused phosphepines **6-8**

Additionally, **6** and **8** were also characterized by X-ray diffraction. They both show similar structural features at the molecular level (Table 1) so the following paragraph will only detail **6**. The P–C bonds lengths are classical for phosphine-like structures ($d_{P-C} = 1.79$ – 1.81 Å). In the 7-membered P-ring, all C–C bonds belonging to the naphthalene moiety are within the aromatic C–C distances (1.42 Å < d < 1.44 Å) while C3–C4 has basically a single bond character ($d = 1.513(5)$ Å). **6** displays a highly distorted C-backbone as illustrated by the C₁₃C₃C₄C₂₀ torsion angle of $38.80(5)^\circ$. The distorted nature of the polycyclic framework in **6-8** is also verified by DFT calculations in the gas phase and the calculated characteristic distances and angles clearly match the experimental data obtained from X-ray diffraction (for details see ESI). Despite the distortion of the backbone, π -dimers ($d = 3.57$ Å) are observed along the b axis in the packing. These dimers are also engaged in π -stacking interactions ($d = 3.73$ Å from phenyl plane to phenyl plane) to form infinite π -columns. **8** also form π -dimers ($d = 3.41$ Å, Fig S17). However, the latter do not self-assemble into π -stacked columns like in the case of **6**.

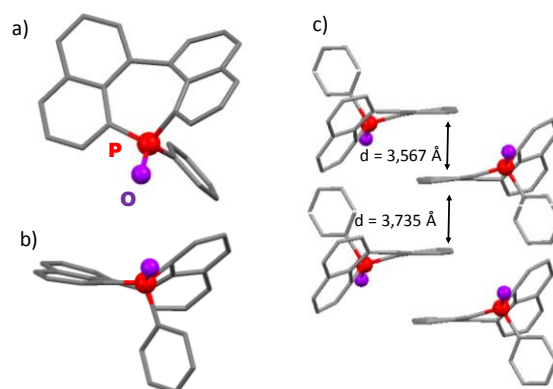


Figure 2: Top (a) and lateral (b) depictions of the X-ray crystal structures of **6**. Columns observed in the packing (c). Hydrogen atoms were omitted for clarity.

Table 1. Characteristic distances and angles taken from X-ray diffraction.

	6	8
P–C ₁ (Å)	1.787 (4)	1.782 (15)
P–C ₆ (Å)	1.801 (4)	1.777 (14)
C ₁ –C ₂ (Å)	1.441 (5)	1.426 (2)
C ₂ –C ₃ (Å)	1.426 (5)	1.441 (2)
C ₃ –C ₄ (Å)	1.513 (5)	1.514 (18)
C ₄ –C ₅ (Å)	1.422 (5)	1.445 (19)
C ₅ –C ₆ (Å)	1.426 (5)	1.435 (2)
C ₁ –P–C ₆ (°)	110.99 (16)	107.54 (7)
C ₁₃ –C ₃ –C ₄ –C ₂₀	38.80 (5)	30.40 (18)

Optical and redox properties

In order to further establish structure-property relationships in this novel family of π -conjugated P-heterocycles **6-8**, their UV-Vis absorption spectra were measured in CH_2Cl_2 (Fig. 3 and Fig. S17), as well as their fluorescence spectra were obtained both in solution and in solid-state and their cyclic voltammetry was measured in DMF with Bu_4NPF_6 as electrolyte (Table 1).

The UV-Vis absorption spectrum of the naphthyl-fused phosphepine **6** consists of a band with an absorption maximum centered at $\lambda_{\text{abs}} = 346 \text{ nm}$ (Fig. 3 and Table 1). This absorption is only weakly modified upon modification of the exocyclic P-R bond (for example, $\Delta\lambda(\mathbf{6-8}) = 5 \text{ nm}$, see Fig. S17 and Table 1). To get more insights into the optical properties of **6-8** TD-DFT calculations have been carried out at the B3LYP/6-31G**/B3LYP/6-31+G* level to obtain vertical excitation energies (see Table 2 for wavelengths and Table S10 for details).^{8b} These calculations confirmed that the main transition observed in UV-Vis absorption is between the HOMO and LUMO orbitals (Table S10). In compounds **6-8** the HOMO and LUMO orbitals are of π and π^* type, respectively (Fig. 3 and Fig S28-29). In these orbitals the electron density is spread over the whole C-backbone, with no contribution of the P-atom in either the HOMO or the LUMO for all the computed structures. Accordingly, the energy of these orbitals shows only a minor change upon substitution (Table 2), clearly explaining why the modification of the P-R bond only weakly affects the UV-Vis absorption. This is in marked differences compared to previously reported 5 or 6 membered P-rings.^{14,6, 14} All phosphepines are good fluorophores with emission in the visible region in diluted solution. For example **6** displays unstructured emission in the visible region ($\lambda_{\text{em}}(\mathbf{6}) = 446 \text{ nm}$, $\phi = 46\%$, Fig 3) with a lifetime of 3 ns, typical for an organic fluorescent emitter (Fig. S21-23). Interestingly, the photophysical properties contrast to the borepin **D** that display a bathochromically shifted absorption ($\lambda_{\text{abs}} = 432 \text{ nm}$) and hypsochromically shifted emission ($\lambda_{\text{em}} = 432 \text{ nm}$, $\phi = 38\%$). This leads to a reduced Stokes shift ($\sigma(\mathbf{6}) = 6841 \text{ cm}^{-1}$; $\sigma(\mathbf{D}) = 1362 \text{ cm}^{-1}$) suggesting a stronger reorganization in the excited state for **6**.¹⁹ The remarkable Stokes shift of **6** is nicely reproduced by the TD-DFT calculations ($\sigma = 6460 \text{ cm}^{-1}$). The optimized geometry of the first excited state (S_1) indeed shows a significant distortion compared to that of the ground state: the plane of the phenyl group is rotated by 49° compared to the O-P- C_{ipso} plane and the $\text{C}_2\text{-C}_3\text{-C}_4\text{-C}_5$ torsional angle increases by 29° (Fig. S30). In addition, naphthyl-fused phosphepines also display luminescence in powder (Fig. 3 and Table 1) as illustrated for **6** that displays emission slightly blue-shifted compared to its emission in diluted solution ($\lambda_{\text{em}}(\mathbf{6}) = 424 \text{ nm}$ with $\phi = 26\%$ Fig. 4). While in solution **6-8** display similar emission wavelength, **8** displays an unexpected behavior in powder with the presence of two maxima ($\lambda_{\text{em}} = 438 \text{ nm}$ and $\lambda_{\text{em}} = 513 \text{ nm}$, Fig. S18). This shift might be due to the formation of different aggregates in the solid-state. Indeed, **6** and **8** display different packing behavior in the crystal (*vide supra*), but an accurate structural comparison cannot be performed as the luminescence is performed on powder samples.

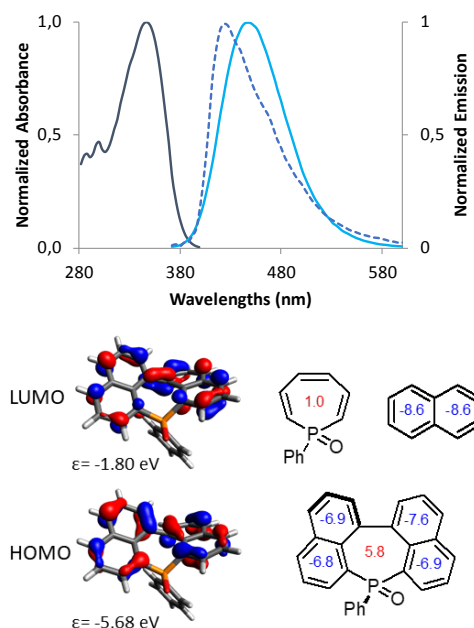


Figure 3: UV-vis absorption (dark blue) and emission (sky blue) in solution and powder (dotted line) of **6** in DCM (up); HOMO and LUMO of **6** calculated at the B3LYP/6-31G**/B3LYP/6-31+G* level (bottom, left); NICS(0) aromaticity patterns of oxa-phosphepine, naphthalene and **6** at the B3LYP/6-311+G**/B3LYP/6-31+G* level (bottom, right).

Regarding the redox properties, **6-8** displays no oxidation processes either in DCM or in DMF. However, a quasi-reversible reduction process is observed around -2.2 V vs Fc in DMF (Fig. S24 and Table 1). As expected, the reduction is not affected when the exocyclic P-R bond is modified, in line with the similar LUMO energies of these compounds (see Table 2). This reduction potential is also similar to the one described for borepin **D**.¹⁹ The aromatic character of the rings in the fused systems **6-8** has been investigated employing Nuclear Independent Chemical Shift (NICS) calculations at the B3LYP/6-311+G**/B3LYP/6-31+G* level (Fig. 3). It is worth mentioning that NICS(0) is a relevant parameter to study the aromaticity of phosphepine as the proximity of the sigma framework does not perturb the NICS(0) value in the case of 6- and 7-membered rings. Furthermore with highly distorted 7-membered rings such as **6**, the actual positions of the Bq atoms for NICS(1) strongly depend on how this plane is defined and this may result in larger changes compared to the NICS(0) values (see ESI). As an example, for **6** the seven-membered ring is anti-aromatic, while the naphthalene moieties of **6** globally retain their characteristic aromatic character.

Table 2. Photophysical and redox data.

	$\lambda_{\text{abs}}^{[a]}$ ($\lambda_{\text{abs}}^{\text{DFT}})^{[b]}$ [nm]	$\epsilon^{[a]}$ [L.mol ⁻¹ .cm ⁻¹]	$\lambda_{\text{em}}^{[a]}$ ($\lambda_{\text{em}}^{\text{DFT}})^{[b]}$ [nm]	$\Phi_{\text{f}}^{[c]}$	τ [ns]	$\lambda_{\text{em}}^{[c]}$ [nm]	$\Phi_{\text{f}}^{[d]}$	$E^{\text{red}}^{[e]}$ [V]	$\epsilon^{\text{HOMO}}^{[b]}$ [eV]	$\epsilon^{\text{LUMO}}^{[b]}$ [eV]
6	346 (357)	14000	446 (464)	0.46	2.9	424	0.26	-2.19 ^[f]	-5.68	-1.80
7	346 (361)	10500	442 (453)	0.46	3.0	432	0.27	-2.20 ^[f]	-5.64	-1.82
8	351 (370)	14000	442 (458)	0.46	2.9	438, 513	0.09	-2.18 ^[f]	-5.65	-1.91

[a] In CH₂Cl₂ (10⁻⁵M). [b] Calculated at the B3LYP/6-31G**/B3LYP/6-31+G* level [c] Measured relative to quinine sulfate (H₂SO₄, 1 N), $\phi_{\text{ref}} = 0.55$. [d] Measured in calibrated integrated sphere. [e] In DMF with Bu₄N⁺PF₆⁻ (0.2 M) at a scan rate of 100 mV.s⁻¹. Potentials vs Fc⁺/Fc. [f] quasi-reversible process.

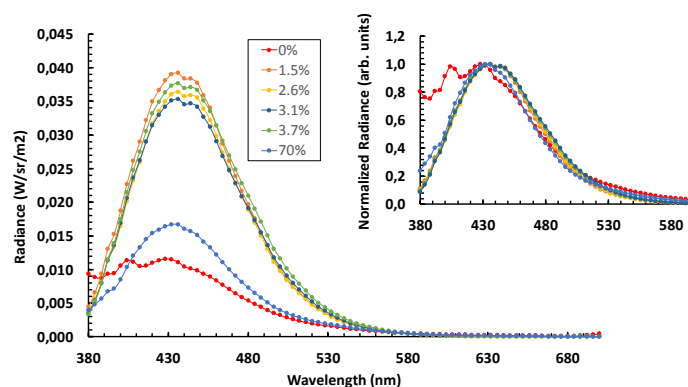
OLEDs devices

Taking in account its thermal stability ($t_{d10} = 338^\circ\text{C}$, Fig S25) and its favorable optical properties, compound **6** was chosen for insertion into multilayer OLED device. However, as no oxidation was recorded, the use of a host matrix having suitable charge transport properties and HOMO-LUMO levels was necessary and 1,3-bis(N-carbazolyl)benzene (mCP) was chosen for this purpose (Fig S26). The performances of the OLED devices are reported in Table 3 and Fig. 4 for different concentrations of **6** in the mCP host. When the mCP matrix is doped with **6**, the emission spectra are changed from emission of mCP (main peak at 404 nm) to the emission of **6** ($\lambda_{\text{em}} = 436$ nm). The devices emit a deep blue color with low CIE (Commission internationale de l'éclairage) color coordinates. Interestingly, the efficiency of the devices is almost independent of the doping rate in the range 1.5 to 3.7% with external quantum efficiency (EQE) of 1.6%. For doping rate as high as 70%, the EQE drops to 0.7% with no significant change of the emission spectrum. This drop can be explained by the low charge transport of **6** which is detrimental to the efficiency of the device. Hence, in these conditions, charge transport is not achieved by the matrix anymore.

Table 3. OLEDs devices performances

Doping ratio [%]	V _{on} ^[a] [V]	EQE ^[b] [%]	cd/A ^[b]	Peak ^[c] [nm]	CIE (x; y) ^[b]
0	4.6	0.7	0.4	404	0.167; 0.110
1.5	4.1	1.6	0.9	436	0.151; 0.075
2.6	4.1	1.6	1.0	436	0.151; 0.077
3.1	4.3	1.5	0.9	436	0.150; 0.083
3.7	4.2	1.6	1.1	436	0.150; 0.086
70	3.7	0.7	0.5	436	0.161; 0.092
Standard deviation	±0.1	±0.05	±0.05	± 4	±0.001

[a] recorded at luminance of 0.1 cd/m² [b] External Quantum efficiency and Current efficiency recorded at 30 mA/cm², [c] main peak.

**Figure 4:** OLEDs spectra recorded at 30 mA/cm² for different doping rates. Insert shows the normalized spectra.

The performance of the best device (2.6% doping rate) is reported in Fig. S27 as a function of the current density. The maximum EQE is 1.65% and the maximum current efficiency is 1 cd/A at 2.5 mA/cm². The EQE drops only by 20% for a current density of 50 mA/cm² in accordance with fluorescent OLEDs. The luminance is proportional to the current density with 400 cd/m² at current density of 50 mA/cm². Despite its modest device performances, these results are highly encouraging as this is, to our knowledge, the first insertion of a phosphine-based emitter in an electroluminescent device. As 4-, 5-, and 6-membered P-rings have already been successfully inserted in OLEDs, these results confirm that π -conjugated P-heterocycles are highly appealing building blocks for lighting purpose.^[1c,5,15]

Conclusions

In conclusion, the straightforward synthesis of a new family of naphthyl-fused phosphines **6-8** has been described. This synthetic approach uses a chlorophosphine-oxide **3** that display strong resistance to hydrolysis due to a combination of steric shielding and pnictogenic interaction. The exocyclic P-R group can be easily tuned using the particular reactivity of **3**, opening the way toward functionalization of the compounds.^[16] These derivatives display a highly distorted polycyclic backbone.

Photophysical studies revealed that these compounds are emissive in solution and in the solid-state. The successful incorporation of **6** into a blue emitting OLED confirmed that organosporous derivatives in general, and π -extended phosphepines in particular, are appealing building blocks to design emitting materials for plastic electronics.

Experimental Section

General procedure. All experiments were performed under argon atmosphere using standard Schlenk techniques. Commercially available reagents were used as received without further purification. Solvents were freshly purified using MBRAUN SPS-800 drying columns. Separations were performed by gravity column chromatography on basic alumina (Aldrich, Type 5016A, 150 mesh, 58 Å) or silica gel (Merck Geduran 60, 0.063-0.200 mm). ^1H , ^{13}C , and ^{31}P NMR spectra were recorded on Bruker AV III 300 and 400 MHz NMR spectrometers equipped with BBO or BBFO probeheads. Assignment of proton and carbon atoms is based on COSY, NOESY, edited-HSQC and HMBC experiments. ^1H and ^{13}C NMR chemical shifts were reported in parts per million (ppm) using residual solvent signal as reference. In the NMR description. High-resolution mass spectra were obtained on a Varian MAT 311 or ZabSpec TOF Micromass instrument at CRMPO (Scanmat, UMS 2001). UV-Visible spectra were recorded on a VARIAN Cary 5000 spectrophotometer. The UV-Vis emission and excitation spectra measurements were recorded on a FL 920 Edinburgh Instrument equipped with a Hamamatsu R5509-73 photomultiplier for the NIR domain (300-1700 nm) and corrected for the response of the photomultiplier. Quantum yields in solution were calculated relative to quinine sulfate (H_2SO_4 , 0.1 M), $\phi_{\text{ref}} = 0.55$. The absolute quantum yields were measured with a C9920-03 Hamamatsu. Fluorescence decay measurements were carried out on the HORIBA Scientific Fluoromax - 4 equipped with its TCSPC pulsed source interface. The electrochemical studies were carried out under argon using an Eco ChemieAutolab PGSTAT 30 potentiostat for cyclic voltammetry with the three-electrode configuration: the working electrode was a platinum disk, the reference electrode was a saturated calomel electrode and the counter-electrode a platinum wire. All potential were internally referenced to the ferrocene/ferrocenium couple. For the measurements, concentrations of 10^{-3} M of the electroactive species were used in freshly distilled and degassed DMF and 0.2 M tetrabutylammoniumhexafluorophosphate. Thermogravimetric Analysis were performed by using a Mettler-Toledo TGA-DSC-1 apparatus under dry nitrogen flow at a heating rate of $10^\circ\text{C}/\text{min}$.

Experimental part. 2. 1,8-Dibromonaphthalene (2 g, 7.1 mmol, 3 eq) is dissolved in 80 mL of dry Et_2O . The solution is cooled down to -80°C then BuLi (2.8 mL, 7.1 mmol, 3 eq) is added dropwise and the solution is stirred for 30 min at -80°C then 30 min at rt. The solution is again cooled down to -80°C and PhPCl_2 (0.423 mg, 2.37 mmol, 1 eq) is added dropwise. The mixture is then stirred at RT overnight. Then the solution is quenched with 16 mL of water. 25 mL of DCM are then added then 4 mL of H_2O_2 . After 2h of stirring, the solution is extracted with water and evaporated. The crude mixture was purified by silica gel chromatography using DCM/ Et_2O (85/15) to afford **2** as a white powder (1.26 g, 99 %) ^1H NMR (400 MHz, CD_2Cl_2 , 243K): 8.11-8.02 (m, 4H), 7.99-7.94 (m, 3H), 7.84 (dd, $J = 8$ Hz, $J = 2$ Hz, 1H), 7.67-7.52 (m, 3H), 7.48-7.30 (m, 6H). ^{13}C NMR (100 MHz, CD_2Cl_2 , 273K): 138.0 (d, $J_{\text{C-P}} = 150$ Hz, C_q), 137.9 (d, $J_{\text{C-P}} = 14$ Hz, CH), 137.4 (d, $J_{\text{C-P}} = 12$ Hz, CH), 137.0 (d, $J_{\text{C-P}} = 7$ Hz, C_q), 135.0 (d, $J_{\text{C-P}} = 60$ Hz, CH), 133.9 (d, $J_{\text{C-P}} = 6$ Hz, CH), 132.6 (d, $J_{\text{C-P}} = 260$ Hz, C_q), 132.4 (d, $J_{\text{C-P}} = 2$ Hz, C_q), 132.4 (s, CH), 131.3 (s, CH), 129.5 (d, $J_{\text{C-P}} = 53$ Hz, CH), 126.8 (d, $J_{\text{C-P}} = 17$ Hz, CH), 124.2 (d, $J_{\text{C-P}} = 15$ Hz, CH), 120.2 (s, C_q). ^{31}P NMR (162 MHz, CD_2Cl_2) δ +42.9. HRMS (ESI, $\text{CH}_3\text{OH} / \text{CH}_2\text{Cl}_2$: 9/1) : $[\text{M}+\text{Na}]^+$ ($\text{C}_{26}\text{H}_{17}\text{ONaBr}_2\text{P}$) m/z Calcd for : 556.9276. m/z Found : 556.9274. Anal. Calcd for $\text{C}_{26}\text{H}_{17}\text{Br}_2\text{OP} \cdot 2\text{H}_2\text{O}$: C, 54.57; H, 3.70. Found: C, 53.77; H, 3.07.

3. 1,8-Dibromonaphthalene (300 mg, 1.06 mmol, 4 eq) is dissolved in 20 mL of dry Et_2O . The solution is cooled down to -80°C then BuLi (0.42 mL, 1.06 mmol, 4 eq) is added dropwise and the solution is stirred for 30 min

at -80°C then 30 min at rt. The solution is again cooled down to -80°C and PCl_3 (37 mg, 0.27 mmol, 1 eq) is added dropwise. The mixture is then stirred at RT overnight. Then the solution is quenched with 4 mL of water. 6 mL of DCM are then added then 1 mL of H_2O_2 . After 2h of stirring, the solution is extracted with water and evaporated. The crude mixture was purified by silica gel chromatography using DCM/ Et_2O (85/15) to afford **3** as a white powder (134 mg, 99 %). ^1H NMR (400 MHz, CD_2Cl_2 , 223K): 8.90 (ddd, $J = 20.1$ Hz, $J = 7.5$ Hz, $J = 2$ Hz, 1H), 8.22-8.13 (m, 2H), 8.09-8.02 (m, 2H), 7.94 (t, $J = 8.1$ Hz, 2H), 7.76-7.69 (m, 2H), 7.47-7.43 (m, 1H), 7.36-7.27 (m, 2H). ^{13}C NMR (100 MHz, CD_2Cl_2 , 223K) δ 137.7 (d, $J = 8.8$ Hz), 136.6 (d, $J = 10.5$ Hz), 136.1 (d, $J = 10.4$ Hz), 135.6 (d, $J = 20.5$ Hz), 135.3 (d, $J = 3.5$ Hz), 135.1 (d, $J = 3.7$ Hz), 131.9 (d, $J = 5.6$ Hz), 129.7 – 129.1 (m), 127.1 (d, $J = 26.2$ Hz), 124.6 (d, $J = 15.8$ Hz), 124.0 (d, $J = 20.5$ Hz), 119.0 (d, $J = 6.0$ Hz). ^{31}P NMR (162 MHz, CD_2Cl_2) δ +51.6. HRMS (ESI, $\text{CH}_3\text{OH} / \text{CH}_2\text{Cl}_2$: 7/3) $[\text{M}+\text{Na}]^+$ ($\text{C}_{20}\text{H}_{12}\text{OCIBr}_2\text{PNa}$) m/z calcd : 514.85732 m/z Found : 514.8572. Anal. Calcd for $\text{C}_{20}\text{H}_{12}\text{Br}_2\text{ClOP}$: found : C, 48.57; H, 2.45. Found: C, 48.04; H, 2.52.

4. (General method A). NaH (129 mg, 3.235 mmol, 4 eq) is dissolved in 40 mL of THF, then EtOH (149 mg, 3.235 mmol, 4 eq) is added at 0°C . After 1.5 h stirring, **3** (400 mg, 0.809 mmol, 1 eq) is added at 0°C , and the reaction is stirred at RT 2 h. Then the solution is quenched with water, extracted with DCM and the solvents were evaporated. The crude mixture was purified by silica gel chromatography using DCM/ Et_2O (9/1) to afford **4** as a white powder (320 mg, 78 %). ^1H NMR (400 MHz, CD_2Cl_2 , 293 K) δ 8.82-7.49 (m, 8H), 7.54-7.34 (m, 4H), 4.19-3.98 (m, 2H), 1.39-1.28 (m, 3H). ^{13}C NMR (101 MHz, CD_2Cl_2) δ 137.2 (s, C_q), 135.4 (s, CH), 134.5 (s, CH), 133.6 (s, C_q), 129.8 (s, CH), 127.0 (s, C_q), 124.9 (d, $J_{\text{C-P}} = 15.8$ Hz, CH), 120.4 (s, C_q), 62.1 (s, CH_2), 16.1 (d, $J_{\text{C-P}} = 1.6$ Hz, CH_3). ^{31}P NMR (162 MHz, CD_2Cl_2) δ +38.0. HRMS (ESI, $\text{CH}_3\text{OH} / \text{CH}_2\text{Cl}_2$: 9/1) $[\text{M}+\text{Na}]^+$ ($\text{C}_{22}\text{H}_{17}\text{O}_2\text{Br}_2\text{NaP}$) m/z Calcd : 524.92251, m/z Found : 524.9224.

5. **5** was synthesized using General Method A with mesitol (396 mg, 2.91 mmol, 4 eq) and **3** (360 mg, 0.78 mmol, 1 eq) to afford **5** as a white powder (320 mg, 78 %). ^1H NMR (400 MHz, CD_2Cl_2) δ 8.69-8.63 (m, 2H), 8.05 (d, 2H, $J = 8.2$ Hz), 7.9 (d, 2H, $J = 8.2$ Hz), 7.76 (d, 2H, $J = 8.2$ Hz), 7.50 (t, 2H, $J = 7.5$ Hz), 7.30 (t, 2H, $J = 7.8$ Hz), 6.81 (s, 2H), 2.24 (s, 3H, Me), 2.06 (s, 6H, Me). ^{13}C NMR (101 MHz, CD_2Cl_2) δ 148.8 (s, C_q), 137.2 (d, $J_{\text{C-P}} = 9.1$ Hz, CH), 137.1 (d, $J_{\text{C-P}} = 10.4$ Hz, C_q), 134.9 (s, CH), 134.4 (d, $J_{\text{C-P}} = 3.4$ Hz, CH), 133.9 (d, $J_{\text{C-P}} = 1.3$ Hz, C_q), 133.6 (d, $J_{\text{C-P}} = 8.1$ Hz, C_q), 133.4 (d, $J_{\text{C-P}} = 142.6$ Hz, C_q), 130.1 (d, $J_{\text{C-P}} = 3.4$ Hz, C_q), 130.0 (s, CH), 129.1 (d, $J_{\text{C-P}} = 2.1$ Hz, CH), 126.9 (s, CH), 125.0 (d, $J_{\text{C-P}} = 15.4$ Hz, CH), 120.1 (d, $J_{\text{C-P}} = 5.1$ Hz, C_q), 20.7 (s, Me), 19.1 (s, Me). ^{31}P NMR (162 MHz, CD_2Cl_2) δ +29.7. HRMS (ESI, $\text{CH}_3\text{OH} / \text{CH}_2\text{Cl}_2$: 9/1) $[\text{M}+\text{Na}]^+$ ($\text{C}_{29}\text{H}_{23}\text{Br}_2\text{NaO}_2\text{P}$) (ESI, $\text{CH}_3\text{OH} / \text{CH}_2\text{Cl}_2$: 90/10) m/z Calcd : 614.96946 m/z Found : 614.9691.

6. (general method B) **2** (200 mg, 0.372 mmol, 1 eq) and 2,2 bipyridine (116 mg, 0.746 mmol, 2 eq) are dissolved in 400 mL of dry THF and degassed for 20 min. COD (0.09, 0.746 mmol, 2 eq) and Ni(COD) $_2$ (206 mg, 0.746 mmol, 2 eq) are added and the solution is stirred overnight at 25°C then 20 mL of MeOH are added. The mixture is filtered on MgSO_4 , washed with Et_2O and the THF is evaporated. The crude mixture was purified by silica gel chromatography using DCM/ AcOEt (1/1) to afford **6** as a white powder (108 mg, 78 %). ^1H NMR (400 MHz, CD_2Cl_2) δ 8.77 (ddd, 2H, $J = 14.4$ Hz, $J = 6.9$ Hz, $J = 1.4$ Hz, H_8), 8.15 (d, 2H, $J = 8.1$ Hz, H_6), 7.95 (d, 2H, $J = 7.7$ Hz, $\text{H}_{2\text{ or }4}$), 7.75 (t, 2H, $J = 7.4$ Hz, H_7), 7.55-7.49 (m, 4H, H_3 and $\text{H}_{2\text{ or }4}$), 7.15-7.11 (m, 1H, H_{para}), 6.95-6.99 (m, 2H, H_{meta}), 6.82-6.77 (m, 2H, H_{ortho}). ^{13}C NMR (101 MHz, CD_2Cl_2) δ 140.1 (d, $J_{\text{C-P}} = 2.0$ Hz, C_1), 137.6 (d, $J_{\text{C-P}} = 118$ Hz, C_{ipso}), 136.1 (s, CH), 134.7 (d, $J_{\text{C-P}} = 4.5$ Hz, C_8), 133.9 (d, $J_{\text{C-P}} = 2.9$ Hz, C_6), 133.8 (d, $J_{\text{C-P}} = 10.1$ Hz, C_5), 132.1 (d, $J_{\text{C-P}} = 11.4$ Hz, C_{10}), 131.0 (d, $J_{\text{C-P}} = 2.3$ Hz, C_{para}), 130.1 (s, CH), 130.1 (d, $J_{\text{C-P}} = 10.4$ Hz, C_{ortho}), 128.5 (d, $J_{\text{C-P}} = 12.1$ Hz, C_9), 128.1 (d, $J_{\text{C-P}} = 12.1$ Hz, C_{meta}), 126.7 (s, CH), 125.6 (d, $J_{\text{C-P}} = 12.1$ Hz, C_7). ^{31}P NMR (162 MHz, CD_2Cl_2) δ +22.7. HRMS (ESI, $\text{CH}_3\text{CN} / \text{CH}_2\text{Cl}_2$: 80/20) $[\text{M}+\text{H}]^+$ ($\text{C}_{26}\text{H}_{18}\text{OP}$) m/z Calcd : 377.10898 m/z Found : 377.1088. Anal. Calcd for $\text{C}_{26}\text{H}_{17}\text{OP}$: C, 82.97; H, 4.55. Found: C, 81.39; H, 4.62.

7. General method B was used using **4** (100 mg, 0.198 mmol, 1 eq) The crude mixture was purified by silica gel chromatography using DCM/ AcOEt (1/1) to afford **7** as a white powder (36 mg, 53 %). ^1H NMR (400 MHz, CD_2Cl_2) δ 8.58 (ddd, 2H, $J = 14.9$ Hz, $J = 6.9$ Hz, $J = 1.5$ Hz, H_8), 8.15 (d, 2H, $J = 8.1$ Hz, H_6), 7.97 (d, 2H, $J = 7.7$ Hz, $\text{H}_{2\text{ or }4}$), 7.69-7.61 (m, 6H, H_7 , H_3 and $\text{H}_{2\text{ or }4}$), 3.03 (q, 2H, $J = 7.2$ Hz, H_{11}), 0.55 (t, 3H, $J = 7.5$ Hz, H_{12}). ^{13}C NMR (101 MHz, CD_2Cl_2) δ 140.5 (d, $J_{\text{C-P}} = 1.9$ Hz, C_q), 136.2 (s, C_7), 134.3 (d, $J_{\text{C-P}} = 3.0$ Hz, C_6), 134.1 (d, $J_{\text{C-P}} = 11.5$ Hz, C_q), 134.1 (d, $J_{\text{C-P}}$

δ = 5.8 Hz, C₈), 132.2 (d, J_{C-P} = 11.6 Hz, C_q), 130.0 (d, J_{C-P} = 1.8 Hz, C_{2or4}), 127.6 (d, J_{C-P} = 129.5 Hz, C₉), 126.8 (s, C_{3or7}), 125.1 (d, J_{C-P} = 13.5 Hz, C_{3or7}), 60.2 (s, CH₂), 15.8 (d, J_{C-P} = 1.6 Hz, CH₃). ³¹P NMR (162 MHz, CD₂Cl₂): δ +27.2. HRMS (ESI, CH₃OH / CH₂Cl₂: 9/1) [M+Na]⁺(C₂₂H₁₇O₂Na) m/z Calcd : 367.0854, m/z Found : 367.0857.

8. General Method B was used with **5** (65 mg, 0.109 mmol, 1 eq) to afford **8** as white powder (38 mg, 47 %). ¹H NMR (400 MHz, CD₂Cl₂) δ 8.58 (ddd, 2H, J = 15.3 Hz, J = 6.9 Hz, J = 1.5 Hz, H₈), 8.19 (d, 2H, J = 8.2 Hz, H₆), 8.00 (d, 2H, J = 8.0 Hz, H_{2 or 4}), 7.75 (d, 2H, J = 7.5 Hz H_{2 or 4}), 7.69-7.64 (m, 4H, H₇ and H₃), 6.58 (s, 2H, H₁₄), 2.10 (s, 3H, H₁₆), 1.33 (s, 6H, H₁₃). ¹³C NMR (101 MHz, CD₂Cl₂) δ 146.5 (s, J_{C-P} = 10.0 Hz, C₁₁), 140.4 (d, J_{C-P} = 1.9 Hz, C_q), 136.4 (s, C_{2 or 4}), 134.5 (d, J_{C-P} = 3.0 Hz, C₆), 134.4 (d, J_{C-P} = 11.6 Hz, C_q), 134.2 (d, J_{C-P} = 2.1 Hz, C_q), 133.4 (d, J_{C-P} = 6.2 Hz, C₈), 132.3 (d, J_{C-P} = 11.7 Hz, C_q), 130.6 (d, J_{C-P} = 3.0 Hz, C_q), 130.1 (d, J_{C-P} = 1.9 Hz, C_{2 or 4}), 129.4 (d, J_{C-P} = 2.0 Hz, C₁₄), 128.2 (s, C_q), 127.0 (s, C_{3 or 7}), 125.2 (d, J_{C-P} = 3.7 Hz, C_{3 or 7}), 20.6 (s, C₁₆), 17.2 (s, C₁₃). ³¹P NMR (162 MHz, CD₂Cl₂) δ + 28.1. HRMS (ESI, CH₃OH / CH₂Cl₂: 9/1) [M+Na]⁺(C₂₉H₂₃O₂Na) m/z Calcd : 457.13279, Found: 457.1311.

X-ray crystallography

Single crystals suitable for X-Ray crystal analysis were obtained by slow diffusion of vapours of pentane into a dichloromethane solution of the derivatives at rt. Single crystal data collection were performed at 150 K with an D8 Venture Bruker-AXS diffractometer with Mo-K α radiation (λ = 0.71073 Å). The structure was solved by dual-space algorithm using the SHELXT program, and then refined with full-matrix least-squares methods based on F²(SHELXL). All non-hydrogen atoms were refined with anisotropic atomic displacement parameters. H atoms were finally included in their calculated positions and treated as riding on their parent atom with constrained thermal parameters.

Computational details.

The computations were performed with the Gaussian 09 program package.^[17] All structures were optimised using the B3LYP, B3LYP/D3 and ω B97XD functionals combined with the 6-31+G* basis set. At each of the optimised structures vibrational analysis was carried out to check that the stationary point located is a minimum of the potential energy hypersurface (no imaginary frequencies were obtained) or a transition state (one imaginary frequency). The minima connected by the transition states were located using intrinsic reaction coordinate (IRC) calculations. The Wiberg Bond Indices were calculated with the NBO program version 3.1.^[18] The AIM analysis was obtained with the Multiwfn code.^[19] The molecular orbitals were plotted with Avogadro program.^[20]

OLEDs fabrication and characterisation

The OLED devices were fabricated onto indium tin oxide (ITO) glass substrates purchased from Xin Yang Technology (90 nm thick, sheet resistance of 15 Ω/\square). Prior to organic layer deposition, the ITO substrates were cleaned by sonication in a detergent solution, rinsed twice in de-ionized water and then in isopropanol solution and finally treated with UV-ozone during 15 minutes. The OLEDs stack used is: Glass / ITO / CuPc (10 nm) / α -NPB (40 nm) / EML (20 nm) / TmPyPB (40 nm) / LiF (1.2 nm) / Al (100 nm). Copper II phthalocyanine (CuPc) is used as hole injection layer (HIL), N, N'-Bis-(1-naphthalenyl)- N,N'-bis-phenyl-(1,1'-biphenyl)-4,4'-diamine (α NPB) as hole transport layer (HTL), 1,3,5-Tri(m-pyridin-3-ylphenyl) benzene, 1,3,5-Tris(3-pyridyl-3-phenyl) benzene (TmPyPB) as electron transport layer (ETL), lithium fluoride as electron injection layer (EIL) and 100 nm of aluminum as the cathode, respectively. The emitting layer (EML) is a host-guest system of 20 nm thick with 1,3-Bis(*N*-carbazolyl)benzene(mCP) as the host and molecule **6** as the guest (doping ratio 0-70% weight). Organic layers were sequentially deposited onto the ITO substrate at a rate of 0.2 nm/s under high vacuum (10⁻⁷ mbar). The doping rate was controlled by simultaneous co-evaporation of the host and the dopant. An in-situ quartz crystal was used to monitor the thickness of the layer depositions with an accuracy of 5%. The active area of the devices defined by the Al cathode was 0.3 cm². The organic layers and the LiF/Al cathode were deposited in a one-step process without breaking the vacuum.

After deposition, all the measurements were performed at rt and under ambient atmosphere with no further encapsulation of devices. The current-voltage-luminance (I-V-L) characteristics of the devices were measured with a regulated power supply (ACT100 Fontaine) combined with a multimeter (Keithley) and a 1 cm² area silicon calibrated photodiode (Hamamatsu). Electroluminescence (EL) spectra and chromaticity coordinates of the devices were recorded with a PR650 SpectraScan spectrophotometer, with a spectral resolution of 4 nm. For each doping rate, 2 devices were prepared (Table S2).

Acknowledgements

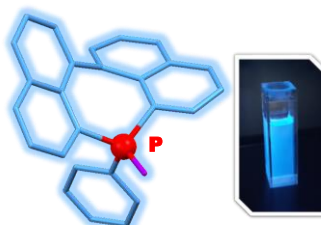
This work is supported by the Ministère de la Recherche et de l'Enseignement Supérieur, the CNRS, the Région Bretagne, the French National Research Agency (ANR Heterographene ANR-16-CE05-0003-01, ANR Fluohyb ANR-17-CE09-0020), OTKA NN 113772 and BME-Nanonotechnology FIKP grant of EMMI (BME FIKP-NAT), PICS SmartPAH (08062)-MTA NKM-44/2019. NKFIH PD 116329, Varga József Alapítvány, Tempus Közalapítvány, János Bolyai Research Fellowship, TÉT_16-1- 2016-0128. The work is supported by the ÚNKP-19-4 New National Excellence Program of the Ministry for Innovation and Technology (ÚNKP-19-4-BME-422). Y. Molard, C. Poriel, C. Quinton (ISCR) and G. Taupier (Scanmat-UMS 2001) are thanked for assistance with luminescence study.

Keywords: π -conjugated systems • P-heterocycles • Optical properties • DFT calculations • OLED

Entry for the Table of Contents

FULL PAPER

Luminescent contorted polycyclic
P-heterocycles



Author(s), Corresponding Author(s)*

Page No. – Page No.

Title

- [1] (a) T. Baumgartner, R. Réau, *Chem. Rev.* **2006**, *106*, 4681-4727. (b) M. Hissler, P. W. Dyer, R. Réau, *Coord. Chem. Rev.* **2003**, *244*, 1-44; (c) D. Joly, P. A. Bouit, M. Hissler, *J. Mater. Chem. C* **2016**, *4*, 3686-3698. (d) M. Stolar, T. Baumgartner, *Chem. As. J.* **2014**, *9*, 1212-1225.
- [2] J. I. Bates, J. Dugal-Tessier, D. P. Gates, *Dalton Trans.* **2010**, *39*, 3151-3159.
- [3](a) P.-A. Bouit, A. Escande, R. Szűcs, D. Szieberth, C. Lescop, L. Nyulászi, M. Hissler, R. Réau, *J. Am. Chem. Soc.* **2012**, *134*, 6524-6527; (b) H. Omori, S. Hiroto, Y. Takeda, H. Fliegl, S. Minakata, H. Shinokubo, *J. Am. Chem. Soc.* **2019**, *141*, 4800-4805.
- [4] (a) F. Mathey, *Chem. Rev.* **1988**, *88*, 429-453; (b) M. P. Duffy, W. Delaunay, P. A. Bouit, M. Hissler, *Chem. Soc. Rev.* **2016**, *45*, 5296-5310; (c) Y. Ren, T. Baumgartner, *Dalton Trans.* **2012**, *41*, 7792-7800; (d) Y. Matano, H. Imahori, *Org. Biomol. Chem.* **2009**, *7*, 1258-1271.
- [5] H. Chen, S. Pascal, Z. Wang, P.-A. Bouit, Z. Wang, Y. Zhang, D. Tondelier, B. Geffroy, R. Réau, F. Mathey, Z. Duan, M. Hissler, *Chem. Eur. J.* **2014**, *20*, 9784-9793.
- [6] (a) C. Müller, L. E. E. Broeckx, I. de Krom, J. J. M. Weemers, *Eur. J. Inorg. Chem.* **2013**, *2013*, 187-202; (b) E. Regulska, C. Romero-Nieto, *Dalton Trans.* **2018**, *47*, 10344-10359.
- [7] (a) X. He, J. Borau-Garcia, A. Y. Y. Woo, S. Trudel, T. Baumgartner, *J. Am. Chem. Soc.* **2013**, *135*, 1137-1147; (b) Y. Ren, M. Sezen, F. Guo, F. Jäkle, Y.-L. Loo, *Chem. Sci.* **2016**, *7*, 4211-4219; (c) W. Winter, *Chem. Ber.* **1976**, *109*, 1405-2419; (d) D. Wu, C. Hu, L. Q. Z. Duan, F. Mathey *Eur. J. Org. Chem.* **2019**, *37*, 6369-6376.
- [8] (a) V. Lyaskovskyy, R. J. A. van Dijk-Moes, S. Burck, W. I. Dzik, M. Lutz, A. W. Ehlers, J. C. Slootweg, B. de Bruin, K. Lammertsma, *Organometallics* **2013**, *32*, 363-373; (b) T. Delouche, A. Mocanu, T. Roisnel, R. Szűcs, E. Jacques, Z. Benkő, L. Nyulászi, P.-A. Bouit, M. Hissler, *Org. Lett.* **2019**, *21*, 802-806.
- [9] K. Schickedanz, J. Radtke, M. Bolte, H.-W. Lerner, M. Wagner, *J. Am. Chem. Soc.* **2017**, *139*, 2842-2851.
- [10] It has been shown that the hydrolysis of the P-Cl bond can be hindered in certain ionic liquids E. Amigues, C. Hardacre, G. Keane, M. Migaud, M. O'Neill, *Chem. Commun.* **2006**, *1*, 72-74.
- [11] Note that similar values have been reported for pnictogen interactions previously: S. Zahn, R. Frank, E. Hey-Hawkins and B. Kirchner, *Chem. Eur. J.* **2011**, *17*, 6034-6038.
- [12] Pnictogen bonding similarly to other so-called σ -hole interactions (hydrogen bond, halogen bond, etc.) is chiefly electrostatic interaction with minor covalent character (charge transfer) arising between a pnictogen center and a Lewis base: (a) S. Scheiner, *Acc. Chem. Res.* **2013**, *46*, 280-288, (b) J. Moilanen, C. Ganesamoorthy, M. S. Balakrishna, H. M. Tuononen, *Inorg. Chem.* **2009**, *48*, 6740-6747. (c) S. Scheiner, Noncovalent forces, Springer, Cham, 2015. (d) V. Lemau de Talancé, M. Hissler, L. Z. Zhang, T. Kárpáti, L. Nyulászi, D. Caras-Quintero, P. Bauerle, R. Réau, *Chem. Commun.* **2008**, 2200-2202.
- [13] Note that the bond path through this BCP erroneously connects the Br and the O atoms (instead of the P atoms) in both **2** and **3**. It has been reported that the bond path tends to connect the more electronegative atoms erroneously and is blind to less electronegative centers: a) M. Jabłoński, *J. Comput. Chem.* **2018**, *39*, 2183-2195. (b) M. Jabłoński, *ChemistryOpen* **2019**, *8*, 497-507
- [14] J. P. Bard, H. J. Bates, C.-L. Deng, L. N. Zakharov, D. W. Johnson, M. M. Haley, *J. Org. Chem.* **2019**, 10.1021/acs.joc.9b02132
- [15] (a) C. Fave, T. Y. Cho, M. Hissler, C. W. Chen, T. Y. Luh, C. C. Wu and R. Réau, *J. Am. Chem. Soc.*, **2003**, *125*, 9254; (b) P. Hindenberg, J. Zimmermann, G. Hernandez-Sosa, C. Romero-Nieto, *Dalton Trans.* **2019**, *48*, 7503-7508.
- [16] Z. Wang, B. S. Gelfand, T. Baumgartner, *Angew. Chem. Int. Ed.* **2016**, *55*, 3481-3485.
- [17] Gaussian 09, Revision E.01, M. J. Frisch, G. W. Trucks, H. B. Schlegel, G. E. Scuseria, M. A. Robb, J. R. Cheeseman, G. Scalmani, V. Barone, B.

Mennucci, G. A. Petersson, H. Nakatsuji, M. Caricato, X. Li, H. P. Hratchian, A. F. Izmaylov, J. Bloino, G. Zheng, J. L. Sonnenberg, M. Hada, M. Ehara, K. Toyota, R. Fukuda, J. Hasegawa, M. Ishida, T. Nakajima, Y. Honda, O. Kitao, H. Nakai, T. Vreven, J. A. Montgomery, Jr., J. E. Peralta, F. Ogliaro, M. Bearpark, J. J. Heyd, E. Brothers, K. N. Kudin, V. N. Staroverov, T. Keith, R. Kobayashi, J. Normand, K. Raghavachari, A. Rendell, J. C. Burant, S. S. Iyengar, J. Tomasi, M. Cossi, N. Rega, J. M. Millam, M. Klene, J. E. Knox, J. B. Cross, V. Bakken, C. Adamo, J. Jaramillo, R. Gomperts, R. E. Stratmann, O.

Yazyev, A. J. Austin, R. Cammi, C. Pomelli, J. W. Ochterski, R. L. Martin, K. Morokuma, V. G. Zakrzewski, G. A. Voth, P. Salvador, J. J. Dannenberg, S. Dapprich, A. D. Daniels, O. Farkas, J. B. Foresman, J. V. Ortiz, J. Cioslowski, and D. J. Fox, Gaussian, Inc., Wallingford CT, 2013
[18] NBO Version 3.1 by E. D. Glendening, A. E. Reed, J. E. Carpenter, F. Weinhold
[19] Lu, T.; Chen, F. *J. Comput. Chem.* **2012**, 33, 580-592
[20] <https://avogadro.cc/>